FRET Conformational Analysis of Calmodulin Binding to Nitric Oxide Synthase Peptides and Enzymes[†]

Donald E. Spratt, Valentina Taiakina, Michael Palmer, and J. Guy Guillemette*

Department of Chemistry, University of Waterloo, Waterloo, Ontario N2L 3G1, Canada

Received July 29, 2008; Revised Manuscript Received September 10, 2008

ABSTRACT: Calmodulin (CaM) is a ubiquitous Ca^{2+}-sensor protein that binds and activates the nitric oxide synthase (NOS) enzymes. We have used fluorescence resonance energy transfer (FRET) to examine the conformational transitions of CaM induced by its binding to synthetic nitric oxide synthase (NOS) CaM-binding domain peptides and full length heme-free constitutive NOS (cNOS) enzymes over a range of physiologically relevant free Ca^{2+} concentrations. We demonstrate for the first time that the domains of CaM collapse when associated with Ca^{2+}-independent inducible NOS CaM-binding domain, similar to the previously solved crystal structures of CaM bound to the Ca^{2+}-dependent cNOS peptides. We show that the association of CaM is not detectable with the cNOS peptides at low free Ca^{2+} concentrations (<40 nM). In contrast, we demonstrate that CaM associates with the cNOS holo-enzymes in the absence of Ca^{2+} and that the Ca^{2+}-dependent transition occurs at a lower free Ca^{2+} concentration with the cNOS holo-enzymes. Our results suggest that other regions outside of the CaM-binding domain in the cNOS enzymes are involved in the recruitment and binding of CaM. We also demonstrate that CaM binds to the cNOS enzymes in a sequential manner with the Ca^{2+}-replete C-lobe binding first followed by the Ca^{2+}-replete N-lobe. This novel FRET study helps to clarify some of the observed similarities and differences between the Ca^{2+}-dependent/independent interaction between CaM and the NOS isozymes.

Calmodulin (CaM[1]) is a ubiquitous cytosolic Ca^{2+}-binding protein that is able to bind and regulate an estimated 300 different intracellular proteins (*1*). CaM consists of two globular domains joined by a central linker region. Each globular domain contains an EF hand pair that is able to bind to Ca^{2+}. The binding of Ca^{2+} to CaM causes the exposure of hydrophobic patches in each globular domain, which allows for CaM to associate to its intracellular target proteins. The inherent flexibility of CaM's central linker separating the N- and C-domains allows it to adapt its conformation to optimally associate with its various intracellular targets (*2*). There is considerable interest in obtaining a better understanding of the structural basis for CaM's ability to bind and recognize its numerous target proteins.

Among the many and varied target proteins bound and regulated by CaM are the nitric oxide synthase (NOS) enzymes (E.C. 1.14.13.39). These enzymes catalyze the production of nitric oxide (•NO), a free radical that acts as a secondary inter- and intracellular messenger involved in many physiological processes (*3, 4*). There are three NOS isozymes found in mammals: neuronal NOS (nNOS, NOS I), endothelial NOS (eNOS, NOS III), and inducible (iNOS, NOS II). The NOS enzymes are homodimeric with each monomer containing an N-terminal oxygenase domain and a C-terminal reductase domain. The oxygenase domain contains binding sites for the catalytic heme, tetrahydrobiopterin (H_4B), and the substrates L-arginine and molecular oxygen, while the reductase domain contains binding sites for the cofactors FMN, FAD, and NADPH (*5*). The oxygenase and reductase domains are connected by a CaM-binding domain. The binding of CaM is required for efficient electron transfer from the reductase to the oxygenase domain for •NO production (*4*). CaM binds and activates the Ca^{2+}-dependent constitutive NOS (cNOS) enzymes, eNOS and nNOS, at elevated cellular Ca^{2+} concentrations. In contrast, iNOS is controlled at the transcriptional level *in vivo* by cytokines and binds to CaM in a Ca^{2+}-independent manner (*5*). The structures of CaM bound to peptides corresponding to the CaM-binding domain of eNOS (*6*) and nNOS (PDB 2O60) have been solved, and it is known that CaM binds to the three NOS enzymes in an antiparallel orientation (*6*−*8*). Although the structures and orientation of CaM bound to cNOS peptides have been determined, the conformation of CaM when bound to all three holo-NOS enzymes has remained elusive. This is due in large part to the size of the

[†] This work was supported by NSERC Grant 183521 (to J.G.G). D.E.S. was the grateful recipient of an Ontario Graduate Scholarship and a UW President's Scholarship.

* Corresponding author. Tel: 519-888-4567ext. 35954. Fax: 519-746-0435. E-mail: jguillem@sciborg.uwaterloo.ca.

[1] Abreviations: Ca^{2+}, calcium ion; Alexa Fluor 546, Alexa Fluor 546 C_5-maleimide; DABMI, 4-dimethylaminophenylazophenyl-4′-maleimide; CaM, calmodulin; CaM-T34C, CaM with threonine 34 mutated to a cysteine; CaM-T110C, CaM with threonine 110 mutated to a cysteine; CaM-T34C-Alexa, CaM-T34C labeled with Alexa Fluor 546; CaM-T110C-Alexa, CaM-T110C labeled with Alexa Fluor 546; NOS, nitric oxide synthase; •NO, nitric oxide; eNOS, endothelial NOS (NOSIII); iNOS, inducible NOS (NOSII); nNOS, neuronal NOS (NOSI); cNOS, constitutive NOS enzymes; NADPH, reduced nicotinamide adenine dinucleotide phosphate; FMN, flavin mononucleotide; FAD, flavin adenine dinucleotide; Heme, protoporphyrin IX; H_4B, (6*R*,6*S*)-2-amino-4-hydroxy-6-(L-erythro-1,2-dihydroxypropyl)-5,6,7,8-tetrahydropterindine; FRET, fluorescence/Förster resonance energy transfer; PCR, polymerase chain reaction; DTT, dithiothreitol; ESI-MS, electrospray ionization-mass spectrometry; QTOF, quadrupole time-of-flight; EDTA, (ethylenedinitro)tetraacetic acid.

10.1021/bi801418s CCC: $40.75
Published on Web 10/24/2008

NOS enzymes (~124−160 kDa per monomer), which prevents their structural determination by NMR spectroscopy, as well as the dynamic structural rearrangements that occur within the reductase domain and CaM-binding domains of the NOS enzymes, which have made it difficult to obtain the protein crystals required to perform X-ray crystallography. There are numerous solved crystal structures of the oxygenase domains for each of the NOS isozymes, as well as a solved crystal structure of the nNOS reductase domain. Because of their highly flexible nature, the autoinhibitory domain and CaM-binding domain were not resolved in the reductase crystal structure (*9*). The conformation of CaM when bound to the NOS enzymes may also be affected by flanking regions outside of the putative CaM-binding domain of each NOS isozyme. For instance, regions in the FMN binding domain of iNOS have been implicated in the Ca^{2+}-independent association of CaM to this enzyme (*10*). Likewise, the autoinhibitory domain and C-terminal tail in the reductase domains of the cNOS enzymes have been shown to be involved in the Ca^{2+}-dependent association of CaM to these enzymes (*11*).

Fluorescence resonance energy transfer (FRET) is a versatile biophysical method with applications ranging from global conformational studies on native proteins *in vivo* to a single protein. It is a useful tool for the determination of the distance between two different fluorescently labeled residues that are ~10 Å to ~100 Å apart (*12*). Since most biological molecules fall within this range, it is not surprising that FRET has been used on a variety of proteins, including CaM. It is well established that CaM is able to interact with its target enzymes in many different conformations, varying from being tightly wrapped when bound to myosin light chain kinase, as determined by NMR (*13*) and X-ray crystallography (PDB 1QS7 and 2O5G), to having an extended structure when bound to the edema factor of adenylyl cyclase from *Bacillus anthracis*, as determined by FRET (*14*) and X-ray crystallography (*15*). The fact that the FRET results of CaM bound to the edema factor were later confirmed by X-ray crystallography validates that the conformation of CaM determined by FRET is representative of its true conformation *in vitro*. Numerous examples of FRET studies using a double cysteine CaM mutant in the N- and C-domains of CaM, specifically at sites T34 and T110 (located in helices 2 and 6 of CaM, respectively), have been reported. These include CaM binding to peptides derived from ryanodine receptor (*17*), Ca^{2+}/CaM-dependent protein kinase II (*18*), and human cardiac L-type Ca^{2+}-voltage gated channel (*18*) as well as the intact edema factor of adenylyl cyclase from *Bacillus anthracis* (*14*). This double-labeled CaM mutant has also been used to monitor CaM's conformation when exposed to various organic, viscous, and denaturing solvents (*19, 20*).

There have been numerous reports on the differences observed in the binding and activation of the NOS enzymes by CaM using a variety of CaM mutants (*21*−*25*). This suggests that there may be a conformational difference in CaM when associated with the Ca^{2+}-dependent cNOS enzymes and the Ca^{2+}-independent iNOS. Furthermore, there have been no reports on the detailed structure of CaM when associated with iNOS. The present study was designed to determine the conformation of CaM when bound to peptides derived from the CaM-binding domains of iNOS and cNOS enzymes, as well as heme-free cNOS at various free Ca^{2+} concentrations through the use of FRET. These results further our present understanding of how CaM is able to associate with mammalian NOS isozymes.

EXPERIMENTAL PROCEDURES

Mutagenesis of CaM to Produce T34C/T110C. The QuikChange site-directed mutagenesis procedure (*26*) was used to convert the threonine codon at position 34 to a cysteine into the kanamycin resistant pCaM-T110C plasmid consisting of the pET9d vector (Novagen) carrying rat calmodulin with a T110C mutation (*7*). The forward and reverse primers for the T34C mutation were wt-T34Cfr and wt-T34Crv, as previously described (*7*). The resulting pCaM-T34C/T110C vector was confirmed by DNA sequencing.

CaM T34C/T110C Expression, Purification, and Fluorescent Labeling. CaM T34C/T110C was expressed and purified as previously described (*23*) with the exception that the dialysis buffer contained 1 mM dithiothreitol (DTT). The CaM protein concentrations were determined using the *DC* Bio-Rad Protein Assay (Bio-Rad Laboratories, Mississauga, ON, Canada) based upon the Lowry method (*27*) and were subsequently frozen in aliquots on dry ice and stored at −80 °C.

Labeling of CaM T34C/T110C was performed in a manner similar to that previously employed for CaM T110C (*7, 28*). CaM T34C/T110C was transferred into labeling buffer (50 mM Tris-HCl and 1 mM EDTA at pH 7.2) by gel filtration using a Sephadex G-25 PD-10 column (Amersham Biosciences) in order to remove excess reducing agent in the CaM sample. Alexa Fluor 546 C_5-maleimide and DABMI (Figure 2) were dissolved in 50 mM Tris at pH 7.5 and *N,N′*-dimethylformamide, respectively, to a concentration of 10 mM; 50 μL of Alexa Fluor 546 and DABMI solutions (500 μM final concentration) were then added to 1 mL of 100 μM CaM T34C/T110C (1.67 mg/mL). The reaction was mixed slowly and allowed to proceed for 2.5 h at room temperature. The labeling reaction was subsequently quenched with the addition of 10 mM DTT. Excess dye and DTT were removed by gel filtration using a PD-10 column pre-equilibrated with 50 mM HEPES, 1 mM EDTA, and 150 mM NaCl at pH 7.5. Dialysis against 50 mM HEPES, 1 mM EDTA, and 150 mM NaCl at pH 7.5 with two changes of buffer were performed to help remove any remaining noncovalently linked dye from the labeled CaM proteins.

The dually labeled CaM T34C/T110C was then purified by reverse-phase chromatography on an AKTApurifier System for Chromatography (Amersham Biosciences, Baie d'Urfe, PQ) using a Vydac 214TP C_4 HPLC column (250 × 4.6 mm, 300 Å pore size, 5 μm particle size). The aqueous mobile phase consisted of 95% (v/v) H_2O, 5% (v/v) CH_3CN, and 0.1% (v/v) TFA, while the organic mobile phase containing 95% (v/v) CH_3CN, 5% (v/v) H_2O, and 0.1% (v/v) TFA was used to elute the dually labeled CaM T34C/T110C protein. The column was washed with two column volumes of the aqueous phase followed by a linear gradient of the organic mobile phase (2.5%/min, up to 30%). The dually labeled CaM proteins (double DABMI, followed by Alexa 546/DABMI, and finally double Alexa 546) were

eluted using a linear gradient of the organic mobile phase (0.4%/min, 30 to 50%). Eluted protein was detected at 278 nm, while DABMI and Alexa Fluor 546 were monitored at 467 and 556 nm, respectively. Double-labeled DABMI CaM T34C/T110C eluted at 39.8% organic mobile phase, followed by dually labeled DABMI/Alexa Fluor 546 CaM at 41.2%, and finally double-labeled Alexa Fluor 546 CaM at 42.3%. Labeling yields were determined from absorbance spectra on a Varian Cary UV−visible Spectrophotometer (Varian, Mississauga, ON). The concentrations of DABMI and Alexa Fluor 546 were determined using $\varepsilon_{419} = 34{,}000\ M^{-1}\ cm^{-1}$ and ε_{554} of 93,000 $M^{-1}cm^{-1}$ (both from Molecular Probes). Isolation of each double- and dually labeled CaM species was confirmed by ESI-MS. CaM T34C and CaM T110C were singly labeled with Alexa Fluor 546 and DABMI as previously described (*7*). The rat nNOS CaM-binding domain peptide was labeled with dabsyl chloride (Figure 2), purified, and characterized as previously described for dabsyl-labeled iNOS peptide (*7*). Labeling was performed in a labeling buffer with a neutral pH (0.1 M $NaCO_3$ at pH 7.1) to ensure the selective labeling of the N-terminus and not the other ε-amines of the lysines found in the nNOS peptide.

Construction of Bovine eNOS C186A and nNOS C415A. Our previous studies have demonstrated that the heme in the NOS enzymes is a potent quencher of Alexa Fluor 546 because of its own fluorescence character and would interfere with FRET measurements (*7*); however, the absence of the heme does not affect the ability of CaM to bind to the NOS enzymes (*29*). Furthermore, the oxidized FMN and FAD cofactors in the reductase domain of NOS absorb poorly in the 550−700 nm range (*30*). Therefore, the CaM−NOS interactions can be examined using the heme-free NOS enzymes.

Using the QuikChange site-directed mutagenesis procedure (*26*), we have mutated the conserved cysteine residue that is axially coordinated to the heme to an alanine to produce heme-free NOS enzymes (nNOS C415A and eNOS C186A), as previously described (*29, 31*). The ampicillin pCWOri vectors with an N-terminal poly histidine tag containing the coding regions for bovine eNOS and rat nNOS were used as the templates for mutagenesis. The forward and reverse primers for the C186A mutation of eNOS involved the incorporation of a unique *Xho*I reporter cut site: eNOSC186Afr 5′ GGCGCAATGCACCTCGA*GCC*GTGGGCCGCATCC-AG 3′ and eNOSC186Arv CTGGATGCGGCCCAC*GGC*TC-GAGGTGCATTGCGCC 3′. The primers used to produce the C415A mutation in nNOS incorporated a *Xho*I site and removed a *BamH*I site: nNOSC415Afr 5′ GGAACGC-CTCTCGA*GCC*GTGGGCA*GA*ATCCAGTGGTCCAAGC 3′ and nNOSC415Arv 5′ GCTTGGACCACTGGAT*TC*TGC-CCAC*GG*CTCGAGAGGCGTTCC 3′. The resulting plas-mids, pCWOri-eNOSC186A and pCWOri-nNOSC415A, were confirmed by DNA sequencing.

Expression and Purification of Heme-Free NOS Enzymes. *E. coli* BL21(DE3) transformed with pCWOri-eNOSC186A and pCWOri-nNOSC415A were used to express bovine eNOS C186A and rat nNOS C415A, respectively, as previously described for the holo-cNOS enzymes (*32, 33*). Purification of the heme-free eNOS and nNOS enzymes involved precipitation with 45% ammonium sulfate followed by metal chelation chromatography. After elution of the protein with 200 mM imidazole, the samples were dialysed as previously described (*32*). The eNOS and nNOS samples were subsequently concentrated using a Vivaspin 15 ultra-filtration spin column (Sartorius AG Biotechnology, Goet-tingen, Germany) to approximately 2 mL to prepare the protein samples for gel filtration. The samples were then loaded onto a HiLoad 16/60 Superdex 200 prep grade column (GE Healthcare Bio-Sciences, Baie d'Urfe, PQ) equilibrated with 50 mM Tris-HCl at pH 7.5, 10% glycerol, 100 mM NaCl, and 1 mM DTT, and 1 mL fractions were collected. The flow rate was maintained at 0.6 mL/min using an AKTApurifier System for Chromatography (GE Healthcare Bio-Sciences), and eluted protein was monitored at 280 nm, while the flavins were monitored at 450 and 480 nm. The nNOS C415A protein that eluted around 54.8 mL, which corresponds to the dimer of nNOS, were collected and pooled. The eNOS C186A protein eluted around 55.6 mL, corresponding to dimeric eNOS, was collected and pooled. The purified heme-free cNOS enzymes were subsequently concentrated using a Vivaspin 15 ultrafiltration spin column and scanned on a Varian Cary UV−visible Spectrophotom-eter. The concentration of the heme-free cNOS proteins was determined using ε_{455} of 15,400 $M^{-1}\ cm^{-1}$ (*34*). The proteins were subsequently aliquoted, flash frozen on dry ice, and stored at −80 °C.

Quin-2 Free Ca^{2+} Concentration Calibration. Steady-state fluorescence measurements were taken in the presence of Quin-2 (Molecular Probes) using the known free Ca^{2+} concentrations at 20 °C. Since physiological concentrations of Ca^{2+} in the cell are low, a calibrated Ca^{2+} buffer kit was also purchased from Molecular Probes with two solutions containing 30 mM MOPS at pH 7.2, 100 mM KCl with either 10 mM K_2EGTA (zero free Ca^{2+}) or 10 mM Ca/EGTA (39 μM free Ca^{2+}), which were prepared using a previously published method (*35*). For increasing free Ca^{2+} concentrations, these buffers were mixed with increasing ratios of Ca/EGTA to K_2EGTA (i.e., 1 mM Ca/EGTA, 2 mM Ca/EGTA, etc.).

The excitation wavelength for Quin-2 was set at 330 nm, and emission was monitored between 400 and 600 nm. Excitation and emission slit widths were set at 1 nm, and the sample was measured at 20 °C. Samples consisted of 1 mL of the mixed Ca/EGTA buffers containing 2 μM Quin-2 in a 1 cm quartz cuvette. The K_d for Quin-2 was determined using the method outlined by Molecular Probes (Product Information C-3008). The experimentally determined K_d for Quin-2 (66 nM) was in good agreement with the previously published K_d for Quin-2 of 60 nM (*35*). Using this curve and K_d, the free Ca^{2+} concentrations were determined for subsequent steady-state and time-resolved fluorescence measurements.

Steady-State Fluorescence Measurements of Alexa-Labeled CaM Proteins with NOS Peptides and Enzymes. Fluorescence emission spectra were obtained using a PTI QuantaMaster spectrofluorimeter. Samples initially contained 50 nM CaM-T34C-Alexa Fluor 546 or Alexa Fluor 546/DABMI T34C/T110C CaM. The excitation wavelength was set at 540 nm, and emission was monitored between 550 and 700 nm. Band passes were set at 2 nm for excitation and 1 nm for emission. In an initial volume of 1 mL, a scan was taken with each CaM protein in a buffer consisting of 50 mM HEPES at pH 7.5, 1 mM EDTA, and 150 mM NaCl. After the initial scan, synthetic NOS CaM-binding domain peptide or heme-free

cNOS enzyme (250 nM) was added to the cuvette, the sample was mixed thoroughly, incubated for three minutes to allow the sample to reach equilibrium, and scanned. The NOS CaM-binding domain peptides for human iNOS, RPKRR EIPLK VLVKA VLFAC MLMRK (residues 507−531), bovine eNOS, TRKKT FKEVA NAVKI SASLM (residues 493−512), and rat nNOS, KRRAI GFKKL AEAVK FSAKL MGQ (residues 725−747) were synthesized by Sigma Genosys (Sigma Aldrich, Mississauga, ON). The sample was then brought to a final free Ca^{2+} concentration calculated to be 0.500 mM, mixed, allowed to incubate for 3 min, and scanned. Finally, excess EDTA (5 mM final) was added and incubated for an additional 3 min, and a final scan was taken. The fluorescence emission maximum of CaM-T34C-Alexa and Alexa/DABMI T34C/T110C CaM was observed at 567 nm, regardless of the presence of Ca^{2+} in the buffer.

Determination of the Förster Distance (R_O) for Alexa Fluor 546 and DABMI Labeled Proteins. To determine the Förster distance (R_O), which is defined as the distance where energy transfer between the donor (Alexa Fluor 546) and acceptor (DABMI) is 50%, steady-state fluorescence of singly labeled Alexa-CaM proteins and absorbance of DAB-labeled CaM proteins were measured in the presence of EDTA and Ca^{2+}. Steady-state fluorescence of CaM-T34C-Alexa and CaM-T110C-Alexa was measured using a PTI QuantaMaster spectrofluorimeter, and emission was monitored from 350−700 nm. The absorbance of CaM-T34C-DAB and CaM-T110C-DAB was measured from 300−700 nm using an Ultrospec 2100 pro UV/vis Spectrophotometer (Biochrom Ltd., Cambridge, UK). The R_O value was determined using a macro programmed for Microsoft Excel entitled SpectraAnalysis (www.science.uwaterloo.ca/~mpalmer/software.html). This macro allows the user to analyze fluorescence or absorbance spectra in a variety of ways including determining the overlap integral, $J(\lambda)$, an important constant involved in the determination of the R_O value for FRET. The overlap integral $J(\lambda)$ was calculated using the following formula:

$$j(\lambda) = \int_0^\infty F_D(\lambda)\varepsilon_A(\lambda)\lambda^4 d\lambda$$

where $F_D(\lambda)$ represents the corrected fluorescence intensity of the donor in the wavelength range of λ to $\lambda + \Delta\lambda$ with the area under the curve normalized, $\varepsilon_A(\lambda)$ represents the extinction coefficient of the acceptor at λ, and λ represents the wavelength in nm (*37*). The overlap integral $J(\lambda)$ is expressed in units of M^{-1} cm^{-1} $(nm)^4$ (*37*).

The R_O value (in Å) was then determined using $J(\lambda)$ in the following formula:

$$R_O = 0.211[\kappa^2 n^{-4} Q_D J(\lambda)]^{1/6}$$

where κ^2 represents the dipole−dipole coupling orientation factor, which is normally assumed to be 2/3; n represents the refractive index of the medium and is normally assumed to be 1.4 for proteins in aqueous solution (*36*); and Q_D represents the quantum yield of the donor and was assumed to be 0.79 for Alexa Fluor 546 (Molecular Probes, probes.invitrogen.com), which can also be determined as previously described (*36, 37*). Using these formulas, the R_O distance was determined to be 31.07 Å in the presence of EDTA and 30.99 Å in the presence of Ca^{2+}. Since both of these values are in good agreement, the assumed R_O used throughout this study was 31 Å. This value correlates well with the theoretical R_O for Alexa Fluor 546 and DABMI of 29 Å (Molecular Probes, probes.invitrogen.com, Table 1.11).

Time-Resolved Fluorescence Measurements of Alexa-Labeled CaM Proteins with NOS Peptides and Enzymes. Time-resolved fluorescence was measured using a PicoQuant FluoTime 100 Compact Fluorescence Lifetime Spectrometer (PicoQuant GmbH, Berlin, Germany) using an LED light source with maximal emission at 500 nm. Settings used on the FluoTime 100 were 50−100% transmittance, source intensity 90, and 520 ± 10 nm bandpass filter. Samples containing 100 nM CaM-T34C-Alexa (Donor alone) and Alexa/DABMI T34C/T110C CaM (Donor/acceptor) were measured in the presence of increasing free Ca^{2+} concentrations (0 to 2 μM). These measurements were taken with labeled CaM alone, as well as in the presence of synthetic NOS peptides or heme-free NOS enzymes (500 nM each). Measurements for CaM-T34C-Alexa and CaM-T110C-Alexa binding to dabsyl-nNOS peptide were performed using the same settings and concentrations as those described for Alexa/DABMI T34C/T110C CaM.

Time-resolved fluorescence decays were analyzed using a homemade program written in Python language and based on the Scientific Python (SciPy) library (www.scipy.org) (Palmer, M., manuscript in preparation). This library supplies implementations of the widely used Levenberg−Marquardt and Nelder−Mead numerical fitting algorithms, which were used for fitting of individual decays and for global fits, respectively. It also supplies a convolution routine, which was used to convolve calculated decays with the instrument response function (IRF); the latter was obtained using a light scatterer with the same light source as that used for the fluorescence measurements. Fitting of individual decays was accomplished using the Levenberg−Marquardt least-squares fitting algorithm. Its SciPy implementation accepts a callback function, which contained both the calculation of the theoretical decay from the current set of parameters and its convolution with the IRF.

In the global fits, a single set of lifetimes was optimized across all included decays so as to minimize the cumulative chi-square value. Global fits were performed using the Nelder−Mead simplex algorithm, and the function whose value was minimized by that algorithm was a wrapper around the single-decay fitting routine described above. For each exploratory set of lifetimes produced by the Nelder−Mead algorithm, all included decays were fitted again individually such that the fractional contributions of each lifetime component were freely variable, whereas the lifetimes were treated as invariant; the average chi-square value resulting from each round of individual fits was then returned to the Nelder−Mead routine to inform its further progress. A detailed description of this program's usage and implementation is available at http://watcut.uwaterloo.ca/trfit.

The experimental data were fitted with single, double, and triple exponential models such that the lifetimes were globally optimized within each related set of experiments, while the fractional contributions of each exponential were freely variable for each individual sample. In addition, global fits were performed, which included all of the samples containing dually labeled CaM. For each data series included in this fit, the fractional contributions of the individual lifetime components were plotted against the free Ca^{2+} concentration and fitted with the Hill

Table 1: Masses of Alexa 546 and DABMI Labeled CaM-Cys Proteins

CaM proteins	mass (Da) [a] observed	mass (Da) [a] theoretical[b]
CaM	16706	16706
CaM T34C	16709	16708
CaM T110C	16709	16708
CaM T34C-Alexa Fluor 546	17718[b]	17720[b]
CaM T110C-Alexa Fluor 546	17718	17720
CaM T34C-DABMI	17027[c]	17029[c]
CaM T110C-DABMI	17027	17029
CaM T34C/T110C-Alexa/DABMI	18041[d]	18040[d]

[a] Masses of deconvoluted ESI-MS spectra were determined with an accuracy of ± 3 Da. [b] Expected mass difference after labeling CaM-Cys proteins with Alexa Fluor 546 C_5-maleimide is 1011.4 Da (Molecular Probes). The manufacturer's MW of the dye is 1034.3, which includes a single counter sodium ion. [c] Expected mass difference after labeling CaM-Cys proteins with DABMI is 320.35 Da (Molecular Probes). [d] Expected mass difference after dual labeling CaM T34C/T110C with Alexa Fluor 546 C_5-maleimide and DABMI is 1331.75 Da (Molecular Probes).

equation. The latter fits were performed with the program Gnuplot (www.gnuplot.info).

FRET Distance Determination for Alexa Fluor 546/DABMI T34C/T110C CaM with NOS Peptides and Enzymes. From the fluorescence lifetimes determined, the energy transfer efficiency (E) was obtained using the following formula:

$$E = 1 - \tau_{DA}/\tau_{D}$$

where τ_{DA} and τ_{D} represent the fluorescent lifetimes for donor−acceptor labeled CaM (Alexa Fluor 546/DABMI T34C/T110C CaM) and donor-labeled CaM (CaM-T34C-Alexa), respectively. Using these energy transfer efficiency (E) values and the R_O value of 31 Å, the FRET distances (R) were calculated using the following formula (expressed in Å):

$$R = R_O[(1 - E)/E]^{1/6}$$

RESULTS

Characterization of Fluorescently Labeled CaM-Cys Proteins. The double cysteine CaM mutant used in this study has been employed extensively in FRET studies focusing on the conformation of CaM alone and in complex with target peptides and proteins (*14, 16, 17, 38*). The positions of residues T34C and T110C in helices 2 and 6 of CaM, respectively, are in close proximity to each other in the classic wrapped conformation, as seen in the CaM-MLCK complex (*13*). In contrast, these residues are markedly separated when CaM is in an extended conformation, as seen in holo-CaM (*39*), apo-CaM (*40*), and CaM in complex with the edema factor from *B. anthracis* (*15*).

The CaM proteins were purified to homogenetity as determined by SDS−PAGE and ESI-MS (Table 1). Fluorescent labeling of CaM T34C, CaM T110C, and CaM T34C/T110C was quantitative and specific, as confirmed by ESI-MS QTOF (Table 1).

Steady-State Fluorescence of Alexa-Labeled CaM Proteins with NOS Peptides and Enzymes. Steady-state fluorescence was used to observe if quenching of the Alexa Fluor 546 by DABMI occurred in the presence of the NOS CaM-binding domain peptides and heme-free cNOS enzymes. Quenching of Alexa Fluor 546 represents the lobes of CaM being in close proximity to each other, while a lack of quenching would represent the lobes being separated. From the previously published CaM-eNOS (*6*) and CaM-nNOS complexes (PDB 2O60), it is apparent that CaM adopts a compact wrapped structure when associated with these peptides and that the T34 and T110 residues are in close proximity to each other. Therefore, it is expected that we should see a marked extent of quenching when the dually labeled CaM is associated with the cNOS peptides. Very little has been reported on the conformation and structure of CaM when associated with iNOS. Although there is some sequence similarity between the cNOS and iNOS CaM-binding domains (Figure 1B), it is possible that CaM may take on a unique conformation when bound to iNOS that differs from the canonical wrapped conformation observed with the cNOS enzymes and MLCK. This is supported by previous studies that have shown major differences in the CaM-dependent binding and activation of the iNOS and cNOS enzymes using a variety of CaM mutant proteins (*21*−*25*).

As in our previous study (*7*), singly labeled CaM-T34C-Alexa showed no fluorescence changes upon the addition of the NOS peptides regardless of Ca^{2+} or EDTA presence, indicating that no quenching of the fluorophore emission occurs when bound to the NOS peptides and enzymes (results not shown). The singly labeled CaM-T34C-Alexa demonstrated a slight quenching (~10%) in the presence of Ca^{2+} and heme-free NOS enzymes (results not shown); however, this quenching was markedly less than what was previously observed with holo-cNOS enzymes (*7*). Although the removal of the heme does not completely stop the quenching of Alexa Fluor 546 fluorescence, quenching was sufficiently reduced to permit FRET measurements.

In contrast to the singly labeled CaM measurements, marked fluorescence changes were observed for dually labeled Alexa/DABMI CaM in the presence of the NOS peptides and enzymes depending on the presence of Ca^{2+} (Figure 3). CaM alone in the presence of EDTA showed little or no quenching, indicating that CaM is in an extended conformation under these conditions. The subsequent addition of Ca^{2+} and NOS peptide or heme-free cNOS enzyme resulted in a dramatic fluorescence decrease, indicating that the dyes are now in close proximity to one another. This marked quenching of fluorescence demonstrates that the domains of CaM collapse when in complex with the NOS peptide and the full-length cNOS enzymes. The final addition of EDTA to the eNOS and nNOS peptides and heme-free enzymes resulted in the return of fluorescence to its original intensity, indicating that CaM releases itself from the peptide and returns to its original extended conformation that also prevails in the absence of NOS peptide. This is in good agreement with previous studies indicating that the interaction between CaM and cNOS peptides is Ca^{2+}-dependent. In contrast, upon addition of EDTA to the CaM-iNOS peptide sample, fluorescence increased slightly but did not return to its original intensity for CaM alone. This shows that CaM is still associated with the iNOS peptide; however, a Ca^{2+}-dependent change in conformation appears to occur as a result of the addition of excess EDTA.

Conformational Analysis of CaM Using Time-Resolved Fluorescence. Time-resolved fluorescence measurements were taken using dually labeled CaM T34C/T110C Alexa/DABMI over a physiological range of free Ca^{2+} concentra-

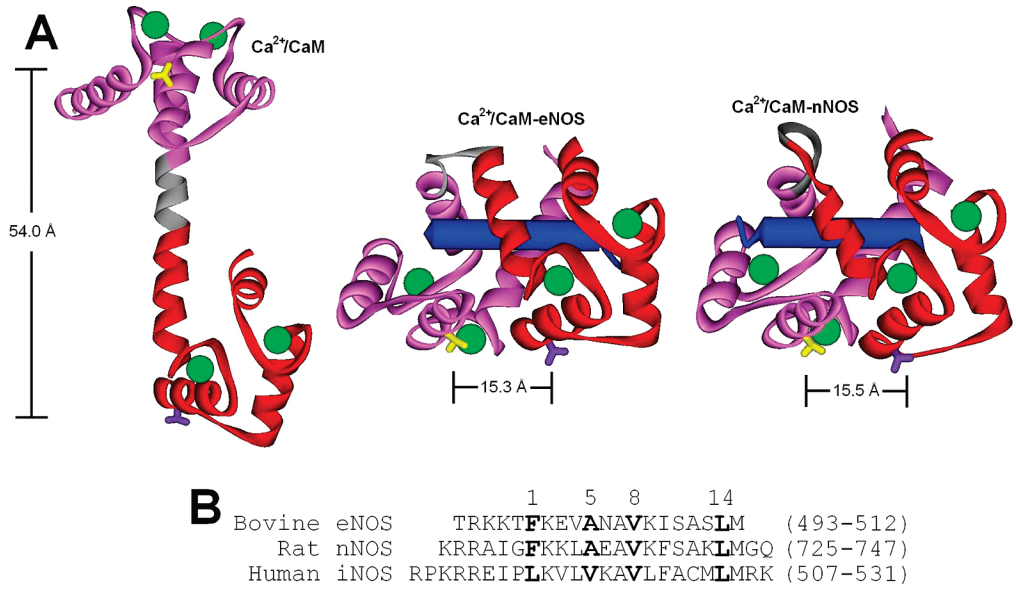

FIGURE 1: X-ray crystal structures showing the positions of T34 and T110 in Ca^{2+}/CaM alone and bound to eNOS and nNOS CaM-binding domain peptides. (A) The distances measured between the hydroxyl groups of T34 and T110 are shown to demonstrate that the dynamic conformational change CaM undergoes when bound to the eNOS and nNOS peptides is amenable to FRET measurements. The N- and C-terminal domains (N-domain = residues 1−75; C-domain = residues 82−148) and central linker (residues 76−81) of CaM are shown in pink, red, and gray, respectively. Ca^{2+} ions are shown in green, and the CaM-target peptides are shown in blue. Models were derived from PDB 1CLL (*39*), 1NIW (*6*) and 2O60 (coordinates released 12−25−2007), respectively, and were visualized using ViewerLite 5.0 (Accelrys). (B) Alignment of the synthetic NOS CaM-binding domain peptides used in this study. Hydrophobic residues typically found in the 1-5-8-14 CaM-binding motif in these peptides are highlighted in bold.

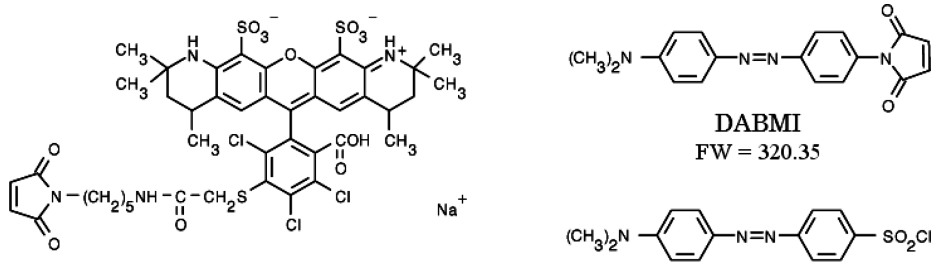

FIGURE 2: Chemical structures of dyes used to label CaM T34C/T110C and nNOS peptide. Alexa Fluor 546 C_5 maleimide, ε_{554} = 93,000 M^{-1} cm^{-1}; $em._{max}$ at 570 nm; DABMI (4-dimethylaminophenylazophenyl-4′-maleimide), ε_{419} = 34,000 M^{-1} cm^{-1}, no emission; dabsyl chloride, ε_{466} = 33,000 M^{-1} cm^{-1}, no emission. Alexa Fluor 546 and DABMI were used to thiol specifically label the cysteine residues in CaM T34C/T110C and were purchased from Molecular Probes. Dabsyl chloride, used to react with the N-terminal amine group of the nNOS peptide, was purchased from Sigma Aldrich.

tions (0 to 2 μM) for (1) CaM alone, (2) CaM with NOS CaM-binding domain peptides, and (3) CaM with the heme-free cNOS enzymes. Singly labeled CaM-T34C-Alexa was used to determine the donor lifetime in the absence of acceptor (τ_D). Any lifetime shorter than τ_D would represent FRET between the donor and the acceptor and could be used to determine the FRET distance between T34 and T110 of CaM in solution. Because of the inherent flexibility of CaM, there are multiple conformations that CaM can undertake, ranging from extended to compact, that are subject to Ca^{2+}-dependent equilibria and the presence of target peptides and proteins. To analyze this conformational variability, we performed a global fit where we fit one, two, and three exponentials to all of the data sets with dual-labeled CaM alone and in the presence of NOS peptides and enzymes (Table 2). This global fitting method involved the lifetimes being globally constrained, while the fractional contributions of each lifetime were allowed to be fully variable for each individual sample. These data sets fit very well with two exponential components with a shorter lifetime and slightly improved with a three exponential fit. In the two exponential fit, there was a longer lifetime corresponding to an extended CaM conformation with a FRET distance of 47 Å, and a shorter lifetime component corresponding to CaM in a compact structure with a FRET distance of 25 Å. The three exponential fit had a longer lifetime virtually identical to the two exponential fit showing very little difference in CaM's extended conformation when analyzed using both fitting methods. The three exponential fit also had two short lifetimes demonstrating some variability of the compact conformation of CaM. This conformational sampling in CaM may be due to variations in CaM's binding to Ca^{2+} and to the target peptides and enzymes; however, a more detailed analysis of these compact forms of CaM is beyond the resolution of the methodology applied here. Therefore, our analysis of CaM binding to the NOS peptides will be reported in terms of two major conformations. CaM in an extended structure and in a compact conformation.

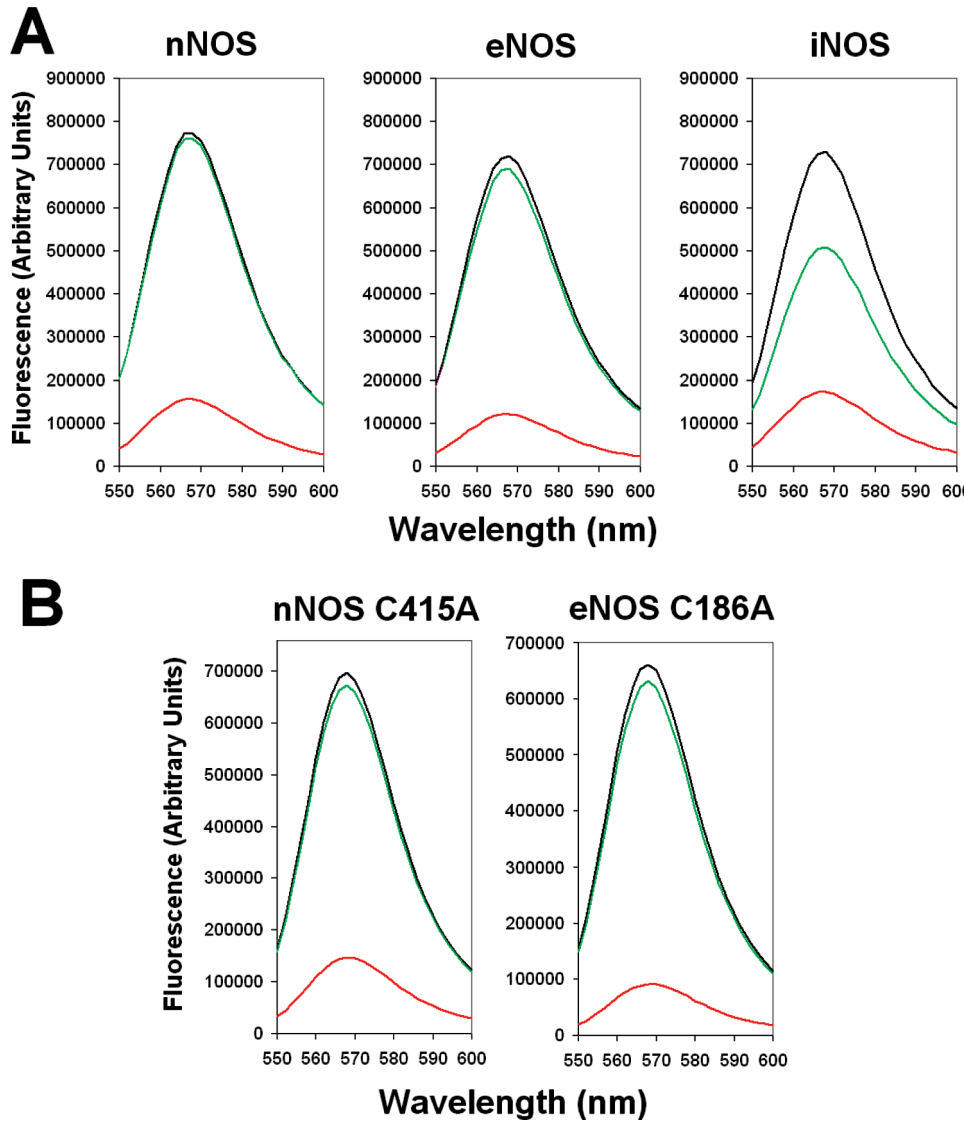

FIGURE 3: Steady-state FRET measurements using Alexa/DABMI labeled CaM T34C/T110C with (A) synthetic NOS CaM-binding domain peptides and (B) heme-free cNOS enzymes. Fluorescence measurements shown were in the presence of EDTA (black line), Ca^{2+} with NOS peptide or enzyme (red line), and EDTA with NOS peptide or enzyme (green line). Excitation was set at 540 nm, and emission was monitored between 550−600 nm.

Table 2: Global Exponential Fits for Dual-Labeled CaM Alone and in the Presence of NOS Peptides and Enzymes

fitting model	lifetime components (ns)	FRET distances (Å)	χ^2
single exponential	2.94	36	11.76
double exponential	0.91,3.76	25, 47	1.29
triple exponential	0.475,1.85.3.90	22,30,52	1.09

We plotted the change in the longer lifetime components' contribution to the fluorescence decay in relation to the free Ca^{2+} concentration when analyzing dual-labeled CaM alone in the presence of NOS peptides and enzymes to determine K_{Ca2+} for each curve (Figure 4). The longer lifetime component was used since it was virtually identical in both the two and three exponential fits. It was apparent from the determined FRET distances that CaM alone is in a predominantly extended conformation (~80%) with a smaller population of CaM being in a compact form (~20%). Interestingly, as the free Ca^{2+} concentration increased, there appears to be very little Ca^{2+}-dependence in the longer and shorter lifetime components in the sample for CaM alone (Figure 4). This demonstrates that any conformational change we observe in the presence of NOS peptides and enzymes is related solely to CaM's association with these target peptide and enzymes. This demonstrates that holo-CaM is predominantly in an extended conformation (Figure 1A) (*40*); however, holo-CaM alone can also be in a closed and compact form, as previously determined by X-ray crystallography (*42*).

Interestingly, the eNOS and nNOS peptide curves are identical to CaM alone at low Ca^{2+} concentrations, indicating that there is no detectable interaction between these molecules at free Ca^{2+} concentrations <40 nM (Figure 4). In contrast, the longer lifetime contribution for dual-labeled CaM in the presence of nNOS C415A was 23% lower than that in the presence of the nNOS peptide, signifying that at low free Ca^{2+} concentrations <10 nM CaM is able to bind or interact with nNOS. Similarly, dual-labeled CaM in the presence eNOS C186A had a longer lifetime contribution of 20% higher than the eNOS peptide at basal Ca^{2+} levels. These results suggest that the cNOS enzymes bind to CaM at low free Ca^{2+} concentrations and have a marked affect

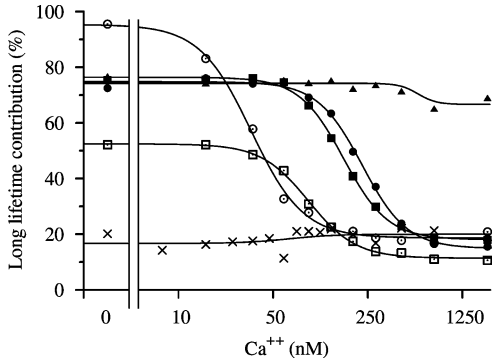

FIGURE 4: Association of Alexa 546/DAB-T34C-T110C CaM to NOS peptides and enzymes with increasing free Ca^{2+} concentrations. Measurements shown represent Alexa 546/DAB-T34C-T110C CaM alone (▲) and in the presence of nNOS peptide (■, 166 ± 4 nM, $h = 2.65$), eNOS peptide (●, 228 ± 7 nM, $h = 2.62$), iNOS peptide (×), nNOS C415A (□, 91 ± 3 nM, $h = 2.48$), and eNOS C186A (•, 35 ± 2 nM, $h = 2.28$). The determined K_{Ca2+} and Hill coefficient (h) for each curve is given in parentheses with the exception of CaM alone and in the presence of iNOS peptide.

on CaM's conformation. In contrast to CaM alone, there was a marked reduction of the longer lifetime component in all of the samples containing either cNOS peptide or enzyme with increasing free Ca^{2+} concentrations representing CaM becoming more compact in complex with the cNOS peptides or enzymes. These samples were fit using the Hill equation to determine the free Ca^{2+} concentration required for the association of CaM to the cNOS peptides and enzymes. The Hill coefficient for each curve in Figure 4 ranged from 2.4 to 2.7 demonstrating that the association of CaM to the cNOS peptides and enzymes is highly cooperative. It is apparent that the eNOS and nNOS peptides require a higher free Ca^{2+} concentration for their association with CaM (eNOS peptide $K_{Ca2+} = 228$ nM; nNOS peptide $K_{Ca2+} = 166$ nM) when compared to that of the full length heme-free eNOS and nNOS, which required lower free Ca^{2+} concentrations for CaM to bind (eNOS C186A $K_{Ca2+} = 35$ nM; nNOS C415A $K_{Ca2+} = 91$ nM). The binding of CaM to the cNOS enzymes at lower free Ca^{2+} concentrations than that for the cNOS peptides can be attributed to the regions flanking the CaM-binding domain of eNOS and nNOS.

In contrast to the Ca^{2+}-dependent curves observed for CaM binding to the cNOS peptides and enzymes, CaM bound to the iNOS peptide had no Ca^{2+}-dependent change in its conformation, and the shorter lifetime component was the predominant species in the sample (Figure 4). Since the observed FRET distance for CaM bound the iNOS peptide is very similar to that observed with the cNOS peptides at higher Ca^{2+} concentrations, CaM apparently binds to iNOS in a tightly wrapped conformation. This result is also consistent with CaM binding to the iNOS peptide in a Ca^{2+}-independent manner and correlates well with our previous fluorescence and spectropolarimetry studies (*7, 22*).

Sequential Binding of CaM Domains to Dabsyl-Labeled nNOS Peptide. To determine the order that CaM's lobes associate with the cNOS CaM-binding domains, we monitored the binding of CaM-T34C-Alexa and CaM-T110C-Alexa to dabsyl-labeled nNOS peptide over the free Ca^{2+} concentration range of 0 to 2 μM. Previous studies with other Ca^{2+}/CaM-dependent enzymes have demonstrated that the Ca^{2+}-replete C-lobe of CaM binds to the target first, and following a subsequent increase in intracellular Ca^{2+} levels, the Ca^{2+}-replete N-lobe binds and activates the enzyme (*42*−*44*). Likewise, we have also observed that there is a sequential association of CaM to nNOS using FRET (Figure 5). We observed only two exponentials for CaM-T34C-Alexa and CaM-T110C-Alexa binding to the dabsyl-nNOS peptide. Figure 5 demonstrates that the shorter lifetime contribution for CaM-T110C-Alexa binding to dabsyl-nNOS peptide of 2.04 ns ($\tau_2 = 4.00$ ns, $\chi^2 = 1.05$), increases at a lower free Ca^{2+} concentration ($K_{Ca2+} = 102$ nM) than that of CaM-T34C-Alexa ($\tau_1 = 1.668$ ns, $\tau_2 = 4.07$ ns, $\chi^2 = 1.08$; $K_{Ca2+} = 340$ nM). This demonstrates that the C-lobe of CaM is able to bind to the nNOS peptide prior to the N-lobe (Figure 5). The free Ca^{2+} concentration for the N-lobe is higher (340 nM) than the binding free Ca^{2+} concentration for dual-labeled CaM with nNOS (172 nM) presented in this study consistent with an increase in the binding affinity of CaM for Ca^{2+} when binding to a target protein (*45*). The affinity of CaM for the nNOS peptide may have been reduced by the dabsyl label. We also observed incomplete labeling of the nNOS peptide with dabsyl chloride by ESI-MS, which would account for the incomplete transition from the longer lifetime to the shorter lifetime component.

DISCUSSION

Although crystal structures of CaM bound to cNOS-target peptides have been solved (Figure 1A), there have been no reported structures for CaM in complex with an iNOS peptide or any regions outside of the CaM-binding domain for all three NOS enzymes. This has been attributed to a high amount of mobility in various regions of the protein, particularly in the reductase domain, making it difficult to form crystals for its structural determination.

The conformational variability of CaM alone and in complex with target peptides and proteins has been studied extensively by X-ray crystallography and NMR spectroscopy. For instance, the crystal structure of holo-CaM has shown an extended conformation with an intact central linker α-helix (*39*); however, a more recent holo-CaM structure demonstrated a closed, compact conformation with the central linker bent, bringing the N- and C-terminal domains into close proximity (*41*). The distance between the T34 and T110 hydroxyl groups is ~54 Å in the extended holo-CaM structure and ~17 Å in the compact holo-CaM structure. As we and others have proven, this large conformational change in CaM alone and in the presence of target peptides and proteins is detectable by FRET (*14, 16*−*20*).

An overview of all released NMR and X-ray crystal structures of CaM alone and in complex with target peptides reveals two common CaM conformations: a wrapped/compact conformation and an extended structure (Table 3). The compact form is more common and includes targets such as MLCK and the cNOS peptides, but there are also some examples of extended conformations including the Ca^{2+} pump and the edema factor from anthrax. To determine the conformation of CaM bound to the iNOS peptide and full length cNOS enzymes, we have used dually labeled CaM T34C/T110C with the FRET donor−acceptor dyes Alexa Fluor 546 C_5-maleimide and DABMI.

The ability of holo-CaM to adopt a variety of conformations has been attributed to the flexible central linker region

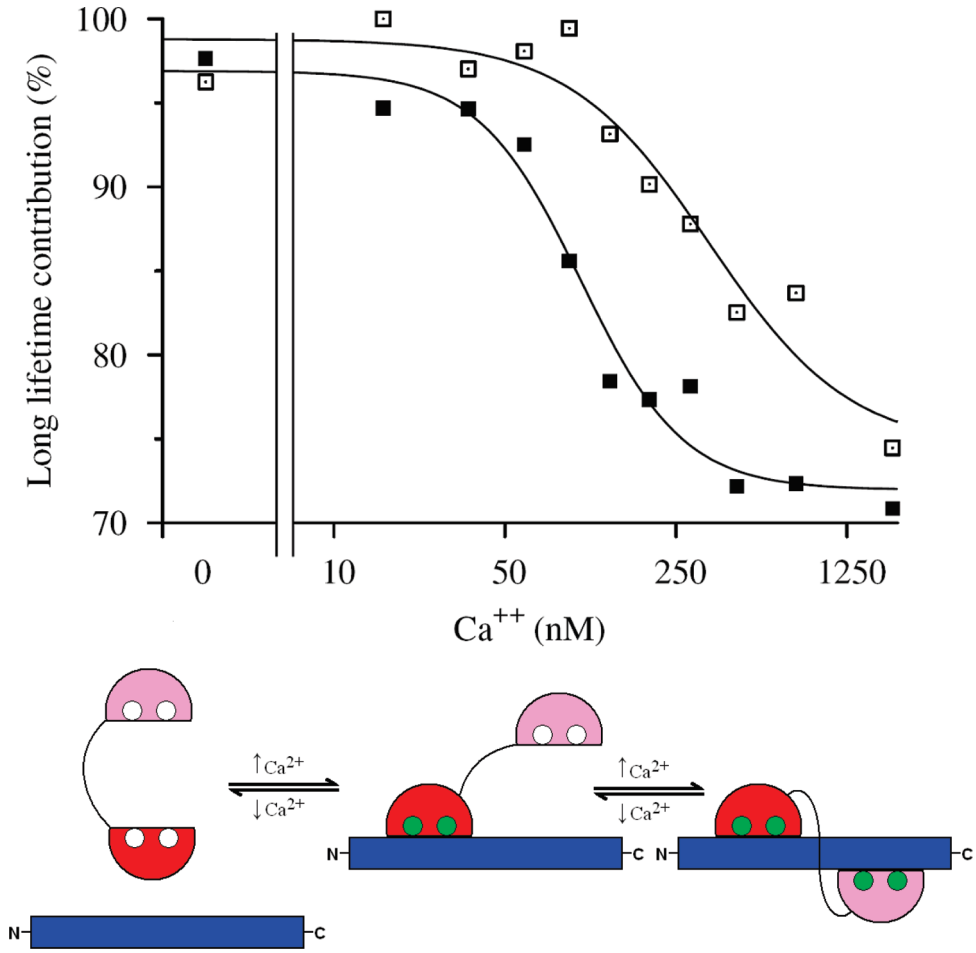

FIGURE 5: Association of CaM T34C-Alexa 546 and CaM T110C-Alexa 546 with dabsyl chloride-labeled nNOS peptide with increasing free Ca^{2+} concentrations. Measurements shown represent dabsyl-labeled nNOS peptide bound to CaM T34C-Alexa (□, 340 nM, $h = 1.51$) and CaM T110C-Alexa (■, 102 nM, $h = 2.07$). The experimentally determined K_{Ca2+} and Hill coefficient (h) for each curve are given in parentheses. The sequential binding of CaM lobes to the CaM-binding domain of nNOS is shown. The N- and C-terminal lobes of CaM are shown in pink and red, respectively. The CaM-binding domain of nNOS is shown in blue. White and green spheres represent lobes in the Ca^{2+}-deplete and -replete conditions. At free [Ca^{2+}] <40 nM, there is no detectable interaction between CaM and the target peptide. At free [Ca^{2+}] between 40 and 200 nM, the Ca^{2+}-replete C-terminal lobe associates with the C-type binding site of the nNOS peptide. At free [Ca^{2+}] > 200 nM, the N-terminal lobe becomes Ca^{2+}-replete and binds to the N-type binding site of the nNOS peptide.

that can unwind, readily bringing the N- and C-lobes of CaM into close proximity with each other. Our results using dually-labeled CaM alone with increasing free Ca^{2+} concentrations are in agreement with a previous FRET study with CaM-dependent protein kinase II (*17*). In this study, they observed only two lifetimes fit their fluorescence decay of a T34C/T110C donor/acceptor labeled CaM, with the predominant species having an amplitude of 75% corresponding to a distance of ~40 Å and the secondary species having an amplitude of 25% and a distance of ~25 Å. Another study demonstrated at a Ca^{2+} concentration of 150 nM a similar ratio of extended to compact forms (*19*).

We have observed a definite trend in the Ca^{2+}-dependent conformation change of CaM associating with the cNOS peptides and enzymes as free Ca^{2+} concentrations increased (Figure 4). The Ca^{2+}-dependent association of CaM occurred at a lower free Ca^{2+} concentration for the cNOS enzymes (~100 nM) than that for the cNOS peptides (~200 nM). Although these K_{Ca2+} values for CaM binding to eNOS C186A and nNOS C415A are lower than previously reported activation profiles for the cNOS enzymes using similar Ca^{2+}/EGTA buffers (*10, 46*−*48*), it is important to note that these previous studies were determining the Ca^{2+} concentration required for NOS activity and not the free Ca^{2+} concentration required for CaM binding to the NOS enzymes. The increase in CaM's affinity for the cNOS enzymes at lower Ca^{2+} concentrations may be related to the various residues found outside of the CaM-binding domain such as the FMN domain itself and possibly the oxygenase domain that have previously been suggested to form contacts with CaM (*4, 10, 11, 21*). Furthermore, although CaM's conformation may be wrapped at a lower concentration of Ca^{2+} than previously reported (*10, 46, 47*), it is important to note that these previous studies were determining the free Ca^{2+} concentration required for NOS activation. It is possible that the Ca^{2+}-replete C-terminal domain of CaM initially binds to the cNOS enzymes causing the initial folding or kinking of CaM into a compact conformation prior to the activation of the enzyme; however, as the Ca^{2+} concentration increases, the N-terminal domain of CaM can become Ca^{2+}-replete, optimally associate to the CaM-binding domain, and fully activate the cNOS enzymes. This is consistent with a previous report that the C-lobe may be weakly associated with nNOS even at Ca^{2+} levels as low as 16 nM using [^{125}I] CaM and that the activation of nNOS involves the sequential binding of CaM's C- and N-terminal domains (*44*). This is further supported by our CaM-T34C-

Table 3: Measured Distances between T34 and T110 in the Solved NMR and X-ray Crystal Structures of CaM Alone and in Complex with CaM Target Peptides and Enzymes

	PDB [a]	compact conformation	distance (Å)[b]	PDB	extended conformation	distance (Å)
CaM	1PRW	compact holo-CaM	17.0	1CFD	apo-CaM	40.3
				1CLL	holo-CaM	54.0
				1Y6W	trapped intermediate of holo-CaM	49.7
CaM-target complex	2O60	neuronal NOS	15.5	1CFF	Ca^{2+}-pump	33.9
	1NIW	endothelial NOS	15.3	1G4Y	SK K^+ channel	32.5
	2BBN	myosin light chain kinase	17.8	1K93	anthrax edema factor	43.4
	1CDM	CaM-dep protein kinase II	17.8	1NWD	glutamate decarboxylase	37.6
	1CKK	CaM-dep kinase kinase (NMR)	16.3	2F2O	calcineurin (fusion)	51.9
	1IQ5	CaM-dep kinase kinase (X-ray)	17.4			52.8
	1IWQ	MARCKS	16.8			
	1L7Z	myristolated CAP-NAP	15.1			
	1MXE	CaM-dep protein kinase I	14.6			
	1SY9	olfactory CNG channel	16.1			
	1YR5	death-associated protein kinase 1	16.6			
	1WRZ	death associated protein kinase 2	15.7			
	1ZUZ	DAPk-related protein kinase 1	16.2			
	2BE6	L-type CaV1.2 IQ domain	15.0			
	3BXL	R-type CaV2.1 IQ domain	16.6			
	3BXK	P/Q-type CaV2.3 IQ domain	16.5			
	2FOT	alpha-II spectrin	13.5			
	2HQW	glutamate NMDA receptor	16.8			
	2BCX	ryanodine receptor	24.1			
	2IX7	apo-CaM with myosin V	20.6			
			19.9			

[a] File was downloaded from the Protein Data Bank (PDB). [b] Measured distance between CaM T34 and T110 hydroxyl groups using ViewerLite 5.0 (Accelrys).

Alexa and CaM-T110C-Alexa binding to dabsyl-labeled nNOS peptide where we observed the sequential association of CaM's C-lobe followed by the N-lobe (Figure 5).

The dually labeled CaM protein had very similar compact FRET distances of 22 Å demonstrating that CaM adopts a compact conformation when bound to the cNOS peptides and enzymes. Although the FRET distances are not equivalent to the measured distance between T34 and T110 hydroxyl groups in the CaM-eNOS and -nNOS crystal structures, taking into account the length of the linker covalently attaching the dyes to the thiols at sites 34 and 110 could account for the ~6 Å difference between the solved crystal structures and our FRET distances (*17*). Another unknown factor in the determination of FRET distances is κ^2, which might have deviated from the assumed value of 2/3.

Interestingly, CaM's conformation when bound to the iNOS peptide appears to be very similar to that of the cNOS peptides. Although the binding and activation of iNOS by CaM differs significantly from cNOS enzymes, our results are not completely surprising since the CaM-binding domains for the three mammalian NOS enzymes show sequence similarity (Figure 1B).

We have previously reported on a subtle Ca^{2+}-dependent conformational change in the C-terminal domain of CaM when bound to iNOS (*7*). To further substantiate this observation, we used the same methodology as in our previous study where we employed an N-terminally labeled iNOS peptide with CaM-T34C-Alexa and CaM-T110C-Alexa in the presence of increasing free Ca^{2+} concentrations. We were unable to observe any Ca^{2+}-dependent changes in CaM and attribute this insensitivity to the longer R_O of the FRET donor−acceptor dyes used in this study. Furthermore, after numerous attempts to monitor the binding of dually-labeled CaM to holo-iNOS, we are unable to report on the conformation of CaM bound to full length iNOS *in vitro* using FRET. This is due the necessity of coexpressing iNOS with CaM, which cannot be displaced from the iNOS CaM-binding domain by our dually-labeled CaM (results not shown). Using the iNOS CaM-binding domain peptide as a working model, we are presently only able to suggest the probable conformation CaM adopts when bound to holo-iNOS.

In conclusion, our results test previous models for CaM's association with the cNOS enzymes and clarify the conformation CaM has when bound to the holo-NOS enzymes. We have observed dynamic conformational changes of CaM alone in solution and in complex with NOS peptides and enzymes by determining the change in FRET distances between N- and C-terminal lobes of CaM. CaM adopts a compact structure when associated with all three NOS CaM-binding domain peptides, demonstrating that the solved crystal structures of CaM bound to cNOS CaM-binding domain peptides are good working models for CaM's conformation when bound to the holo-cNOS enzymes. Since previous reports have shown that regions flanking the CaM-binding domain in NOS can interact with CaM, such as the autoinhibitory domain and FMN domain itself (*10, 21, 48*), FRET measurements were performed with peptides and holo-NOS enzymes to determine if there were any significant differences in CaM's conformation due to these regions outside of the CaM-binding domain. There appears to be no significant difference in the conformation of CaM when bound to cNOS peptides and holo-cNOS enzymes; however, the eNOS and nNOS enzymes differ in their effect on the conformational equilibrium of CaM when bound at lower Ca^{2+} concentrations. Furthermore, our novel FRET studies demonstrate for the first time that the domains of CaM collapse when bound to the CaM-binding domain of iNOS, very similar to the conformation of CaM bound to the cNOS

enzymes. By determining the conformation and the effect of free Ca^{2+} concentrations on the association of CaM to the three NOS enzymes, we have expanded and clarified the present understanding of the CaM-dependent binding and activation of the mammalian NOS enzymes.

REFERENCES

1. Ikura, M., and Ames, J. B. (2006) Genetic polymorphism and protein conformational plasticity in the calmodulin superfamily: two ways to promote multifunctionality. *Proc. Natl. Acad. Sci. U.S.A. 103*, 1159–1164.
2. Ishida, H., and Vogel, H. J. (2006) Protein-peptide interaction studies demonstrate the versatility of calmodulin target protein binding. *Protein Pept. Lett. 13*, 455–465.
3. Alderton, W. K., Cooper, C. E., and Knowles, R. G. (2001) Nitric oxide synthases: structure, function and inhibition. *Biochem. J. 357*, 593–615.
4. Ghosh, D. K., and Salerno, J. C. (2003) Nitric oxide synthases: domain structure and alignment in enzyme function and control. *Front. Biosci. 8*, d193–209.
5. Roman, L. J., Martasek, P., and Masters, B. S. (2002) Intrinsic and extrinsic modulation of nitric oxide synthase activity. *Chem. Rev. 102*, 1179–1190.
6. Aoyagi, M., Arvai, A. S., Tainer, J. A., and Getzoff, E. D. (2003) Structural basis for endothelial nitric oxide synthase binding to calmodulin. *EMBO J. 22*, 766–775.
7. Spratt, D. E., Taiakina, V., Palmer, M., and Guillemette, J. G. (2007) Differential binding of calmodulin domains to constitutive and inducible nitric oxide synthase enzymes. *Biochemistry 46*, 8288–8300.
8. Zhang, M., Yuan, T., Aramini, J. M., and Vogel, H. J. (1995) Interaction of calmodulin with its binding domain of rat cerebellar nitric oxide synthase. A multinuclear NMR study. *J. Biol. Chem. 270*, 20901–20907.
9. Garcin, E. D., Bruns, C. M., Lloyd, S. J., Hosfield, D. J., Tiso, M., Gachhui, R., Stuehr, D. J., Tainer, J. A., and Getzoff, E. D. (2004) Structural basis for isozyme-specific regulation of electron transfer in nitric-oxide synthase. *J. Biol. Chem. 279*, 37918–37927.
10. Ruan, J., Xie, Q., Hutchinson, N., Cho, H., Wolfe, G. C., and Nathan, C. (1996) Inducible nitric oxide synthase requires both the canonical calmodulin-binding domain and additional sequences in order to bind calmodulin and produce nitric oxide in the absence of free Ca2+. *J. Biol. Chem. 271*, 22679–22686.
11. Roman, L. J., and Masters, B. S. (2006) Electron transfer by neuronal nitric-oxide synthase is regulated by concerted interaction of calmodulin and two intrinsic regulatory elements. *J. Biol. Chem. 281*, 23111–23118.
12. Heyduk, T. (2002) Measuring protein conformational changes by FRET/LRET. *Curr. Opin. Biotechnol. 13*, 292–296.
13. Ikura, M., Clore, G. M., Gronenborn, A. M., Zhu, G., Klee, C. B., and Bax, A. (1992) Solution structure of a calmodulin-target peptide complex by multidimensional NMR. *Science 256*, 632–638.
14. Drum, C. L., Yan, S. Z., Sarac, R., Mabuchi, Y., Beckingham, K., Bohm, A., Grabarek, Z., and Tang, W. J. (2000) An extended conformation of calmodulin induces interactions between the structural domains of adenylyl cyclase from Bacillus anthracis to promote catalysis. *J. Biol. Chem. 275*, 36334–36340.
15. Drum, C. L., Yan, S. Z., Bard, J., Shen, Y. Q., Lu, D., Soelaiman, S., Grabarek, Z., Bohm, A., and Tang, W. J. (2002) Structural basis for the activation of anthrax adenylyl cyclase exotoxin by calmodulin. *Nature 415*, 396–402.
16. Maximciuc, A. A., Putkey, J. A., Shamoo, Y., and Mackenzie, K. R. (2006) Complex of calmodulin with a ryanodine receptor target reveals a novel, flexible binding mode. *Structure 14*, 1547–1556.
17. Torok, K., Tzortzopoulos, A., Grabarek, Z., Best, S. L., and Thorogate, R. (2001) Dual effect of ATP in the activation mechanism of brain Ca(2+)/calmodulin-dependent protein kinase II by Ca(2+)/calmodulin. *Biochemistry 40*, 14878–14890.
18. Xiong, L., Kleerekoper, Q. K., He, R., Putkey, J. A., and Hamilton, S. L. (2005) Sites on calmodulin that interact with the C-terminal tail of Cav1.2 channel. *J. Biol. Chem. 280*, 7070–7079.
19. Slaughter, B. D., Unruh, J. R., Allen, M. W., Bieber Urbauer, R. J., and Johnson, C. K. (2005) Conformational substates of calmodulin revealed by single-pair fluorescence resonance energy transfer: influence of solution conditions and oxidative modification. *Biochemistry 44*, 3694–3707.
20. Slaughter, B. D., Unruh, J. R., Price, E. S., Huynh, J. L., Bieber Urbauer, R. J., and Johnson, C. K. (2005) Sampling unfolding intermediates in calmodulin by single-molecule spectroscopy. *J. Am. Chem. Soc. 127*, 12107–12114.
21. Newman, E., Spratt, D. E., Mosher, J., Cheyne, B., Montgomery, H. J., Wilson, D. L., Weinberg, J. B., Smith, S. M., Salerno, J. C., Ghosh, D. K., and Guillemette, J. G. (2004) Differential activation of nitric-oxide synthase isozymes by calmodulin-troponin C chimeras. *J. Biol. Chem. 279*, 33547–33557.
22. Spratt, D. E., Taiakina, V., and Guillemette, J. G. (2007) Calcium-deficient calmodulin binding and activation of neuronal and inducible nitric oxide synthases. *Biochim. Biophys. Acta 1774*, 1351–1358.
23. Spratt, D. E., Newman, E., Mosher, J., Ghosh, D. K., Salerno, J. C., and Guillemette, J. G. (2006) Binding and activation of nitric oxide synthase isozymes by calmodulin EF hand pairs. *FEBS J. 273*, 1759–1771.
24. Gribovskaja, I., Brownlow, K. C., Dennis, S. J., Rosko, A. J., Marletta, M. A., and Stevens-Truss, R. (2005) Calcium-binding sites of calmodulin and electron transfer by inducible nitric oxide synthase. *Biochemistry 44*, 7593–7601.
25. Stevens-Truss, R., Beckingham, K., and Marletta, M. A. (1997) Calcium binding sites of calmodulin and electron transfer by neuronal nitric oxide synthase. *Biochemistry 36*, 12337–12345.
26. Wang, W., and Malcolm, B. A. (1999) Two-stage PCR protocol allowing introduction of multiple mutations, deletions and insertions using QuikChange Site-Directed Mutagenesis. *Biotechniques 26*, 680–682.
27. Lowry, O. H., Rosebrough, N. J., Farr, A. L., and Randall, R. J. (1951) Protein measurement with the Folin phenol reagent. *J. Biol. Chem. 193*, 265–275.
28. Lang, S., Spratt, D. E., Guillemette, J. G., and Palmer, M. (2005) Dual-targeted labeling of proteins using cysteine and selenomethionine residues. *Anal. Biochem. 342*, 271–279.
29. Richards, M. K., Clague, M. J., and Marletta, M. A. (1996) Characterization of C415 mutants of neuronal nitric oxide synthase. *Biochemistry 35*, 7772–7780.
30. Munro, A. W., and Noble, M. A. (1999) Fluorescence analysis of flavoproteins. *Methods Mol. Biol. 131*, 25–48.
31. Chen, P. F., Tsai, A. L., and Wu, K. K. (1994) Cysteine 184 of endothelial nitric oxide synthase is involved in heme coordination and catalytic activity. *J. Biol. Chem. 269*, 25062–25066.
32. Roman, L. J., Sheta, E. A., Martasek, P., Gross, S. S., Liu, Q., and Masters, B. S. (1995) High-level expression of functional rat neuronal nitric oxide synthase in Escherichia coli. *Proc. Natl. Acad. Sci. U.S.A. 92*, 8428–8432.
33. Martasek, P., Liu, Q., Liu, J., Roman, L. J., Gross, S. S., Sessa, W. C., and Masters, B. S. (1996) Characterization of bovine endothelial nitric oxide synthase expressed in *E. coli*. *Biochem. Biophys. Res. Commun. 219*, 359–365.
34. Newton, D. C., Montgomery, H. J., and Guillemette, J. G. (1998) The reductase domain of the human inducible nitric oxide synthase is fully active in the absence of bound calmodulin. *Arch. Biochem. Biophys. 359*, 249–257.
35. Tsien, R., and Pozzan, T. (1989) Measurement of cytosolic free Ca2+ with quin2. *Methods Enzymol. 172*, 230–262.
36. Lakowicz, J. R. (2006) *Principles of Fluorescence Spectroscopy*, 3rd ed., Springer, New York, NY.
37. Van der Meer, B. W., Coker, G., and Chen, S. Y. S. (1994) *Resonance Energy Transfer: Theory and Data*, VCH, New York, NY.
38. Allen, M. W., Urbauer, R. J., Zaidi, A., Williams, T. D., Urbauer, J. L., and Johnson, C. K. (2004) Fluorescence labeling, purification, and immobilization of a double cysteine mutant calmodulin fusion protein for single-molecule experiments. *Anal. Biochem. 325*, 273–284.
39. Chattopadhyaya, R., Meador, W. E., Means, A. R., and Quiocho, F. A. (1992) Calmodulin structure refined at 1.7 A resolution. *J. Mol. Biol. 228*, 1177–1192.
40. Kuboniwa, H., Tjandra, N., Grzesiek, S., Ren, H., Klee, C. B., and Bax, A. (1995) Solution structure of calcium-free calmodulin. *Nat. Struct. Biol. 2*, 768–776.
41. Fallon, J. L., and Quiocho, F. A. (2003) A closed compact structure of native Ca(2+)-calmodulin. *Structure 11*, 1303–1307.
42. Persechini, A., McMillan, K., and Leakey, P. (1994) Activation of myosin light chain kinase and nitric oxide synthase activities by calmodulin fragments. *J. Biol. Chem. 269*, 16148–16154.

43. Sun, H., and Squier, T. C. (2000) Ordered and cooperative binding of opposing globular domains of calmodulin to the plasma membrane Ca-ATPase. *J. Biol. Chem. 275*, 1731–1738.
44. Weissman, B. A., Jones, C. L., Liu, Q., and Gross, S. S. (2002) Activation and inactivation of neuronal nitric oxide synthase: characterization of Ca(2+)-dependent [125I]Calmodulin binding. *Eur. J. Pharmacol. 435*, 9–18.
45. Olwin, B. B., and Storm, D. R. (1985) Calcium binding to complexes of calmodulin and calmodulin binding proteins. *Biochemistry 24*, 8081–8086.
46. Nishida, C. R., and Ortiz de Montellano, P. R. (1999) Autoinhibition of endothelial nitric-oxide synthase. Identification of an electron transfer control element. *J. Biol. Chem. 274*, 14692–14698.
47. Montgomery, H. J., Romanov, V., and Guillemette, J. G. (2000) Removal of a putative inhibitory element reduces the calcium-dependent calmodulin activation of neuronal nitric-oxide synthase. *J. Biol. Chem. 275*, 5052–5058.
48. Nishida, C. R., and de Montellano, P. R. (2001) Control of electron transfer in nitric-oxide synthases. Swapping of autoinhibitory elements among nitric-oxide synthase isoforms. *J. Biol. Chem. 276*, 20116–20124.
49. Venema, R. C., Sayegh, H. S., Kent, J. D., and Harrison, D. G. (1996) Identification, characterization, and comparison of the calmodulin-binding domains of the endothelial and inducible nitric oxide synthases. *J. Biol. Chem. 271*, 6435–6440.

BI801418S